AIMS Materials Science, 8(4): 640–658.
DOI: 10.3934/matersci.2021039
Received: 25 June 2021
Accepted: 31 August 2021
Published: 01 September 2021

http://www.aimspress.com/journal/Materials

Research article

Preparation and characterization of novel environmentally sustainable mortars based on magnesium potassium phosphate cement for additive manufacturing

Stelladriana Volpe[1], Andrea Petrella[1], Valentino Sangiorgio[1,2,3], Michele Notarnicola[1] and Francesco Fiorito[1,*]

[1] DICATECH, Dipartimento di Ingegneria Civile, Ambientale, del Territorio, Edile e di Chimica, Politecnico di Bari, Via Edoardo Orabona 4, Bari, Italy
[2] ICITECH, Universitat Politècnica de València, Camí de Vera, s/n, 46022 València, Spain
[3] FEUP, Faculdade de Engenharia da Universidade do Porto, R. Dr. Roberto Frias, 4200-465 Porto, Portugal

* **Correspondence:** Email: francesco.fiorito@poliba.it; Tel: +39 080 5963401.

Abstract: The "Digital Transition" of the building sector and in particular the concrete 3D printing is profoundly changing building technologies and construction processes. However, the materials engineering is still a challenge for the research of even more effective and performing 3D printable concrete. In this context, we analysed magnesium potassium phosphate cement (MKPC) performance as an innovative cementitious material in terms of sustainability and possibility of its use in extrusion-based 3D concrete printing (3DPC). Starting from common formulations present in literature, we discussed the relationship between water to binder ratio and workability in two different quantities of retarders. Some mix compositions were also prepared by replacing sand with rubber aggregates or glass aggregates with the aim of creating lightweight aggregate-based mortars. In addition, the fly ash (FA), a widely material used (but that will not be available in the next few years), was replaced with silica fume (SF). We found that two formulations (samples 2 and 7) show rheological requirements and compressive strengths at 90 min of respectively about 2 MPa and 3 MPa, which are deemed to be suitable for 3D printing processes. Moreover, in sample 7, the use of the expanded recycled glass as aggregate opens new possibilities for reducing the carbon footprint of the process.

Keywords: magnesium potassium phosphate cement; 3D concrete printing; sustainable cement; printable concrete; specimens; compressive strength; flexural strength

1. Introduction

During the 20th century, the construction industry was almost based on the use of Portland cement (PC) [1]. This globalisation led to a loss of interest in other materials and construction techniques even if the Portland cement production is responsible of 5–8% of carbon dioxide emission of the world [2]. Nowadays with the growing debate on sustainability, the construction sector is evolving towards more sustainable alternatives. In particular, the 3D printing of concrete is one of the most promising technologies and is changing the whole construction process [3]. In parallel to the diffusion of 3D concrete printer, the research interest in a possible environmentally friendly alternative to Portland cement (suitable for 3D printing) is emerging. An interesting possibility is offered using phosphate cements, derived from reactions between phosphate and metal oxide.

Among them, magnesium phosphate cement (MPC) is a type of binder formed by the reaction between phosphate and dead burnt magnesia [4]. It was first developed as dental cement [5] and in other medical application for its compatibility with human body [6]. On the other hand, important advantages can be found in the construction sector. In the last years, magnesium phosphate composites have been employed in constructions for rapid structural repairs [7,8], in cement-based pavements [9], and for the treatment of dangerous wastes. All these applications have been made possible due to positive characteristics of MPCs in terms of hydration process, high early strength, good durability, and stabilisation of hazardous materials (toxic, nuclear wastes, heavy-metal contaminants) [10,11,1,12].

Beyond the classical applications, MPC has numerous advantages which make it particularly interesting in the use as 3D printable material [13]. Indeed, the most promising MPC characteristics for the application in the additive manufacturing are (i) quick setting time, (ii) high early strength, iii) setting in a low temperature environment, (iv) bonding strength between concrete layers, (v) resistance to abrasion and frost, (vi) low drying shrinkage, (vii) fireproof behaviour, and viii) low thermal expansion coefficient [2]. On the other hand, even if the MPC has a great potential in the concrete 3D printing technology, there are only some preliminary investigations to achieve a 3D printable material with this type of cement [13]. In particular, the correct chemical admixture to reach a perfect balance among viscosity (extrudability), setting time, compressive and flexural strength are missing in related literature. Beyond this, the most of the MPCs have the criticality of the presence of "fly ash" in the composition of the conglomerates: a material that will be unavailable in large quantities in the future.

The different printable mixtures must meet specific requirements of extrudability, viscosity, and workability [14]. The available literature of the last years on 3D printable materials investigated the mechanical properties and the printability optimisation incorporating different kind of additive like geopolymers [15,16], polypropylene fibres [17], poly-vinyl alcohol fibres [18], glass fibre [19] or steel fibre [20]. Another important aspect regards the substitution of aggregates with waste materials that could deeply influence the rheological, thermal and mechanical properties [21].

This study investigates different chemical admixtures with magnesium potassium phosphate cement (MKPC) in order to identify the best composition to guarantee the most important 3D

printable material characteristics by also considering the sustainability of the production and reduction of raw materials consumption. An objective of the experimentation is to reach a mortar with flowability results between 20% and 60% to be also suitable for 3D printing. At the same time, the mechanical resistance should be sufficient to allow extrusion.

Therefore, we have proposed and tested four different groups of samples (twelve different chemical admixtures) to investigate the best compositions in terms of viscosity, setting time, compressive and flexural strength. The samples were prepared starting from the ratios of the mix composition M40FA60S10-4 used in a preliminary study [13], evaluating and improving different properties. Among the proposed chemical admixtures, two compositions turned out to be performing and advisable for the use with the additive manufacturing technology.

The novelty of the proposed research is threefold:

(I) A novel chemical admixture with lightweight aggregates and good performances in 3D printing has been found and tested.

(II) An alternative composition is proposed to substitute the "fly ash" in the chemical admixture by maintaining the same performance of traditional MPC.

(III) Specific guidelines are developed to support stakeholders and technicians in the practical development of the two best MKPC compositions among the twelve samples investigated.

2. Magnesium phosphate cements

Ammonium phosphate $NH_4H_2PO_4$ is generally used in MPC production, but it can be also replaced by potassium dihydrogen phosphate KH_2PO_4 [8]. KH_2PO_4 has a reduced acidity, that yields a slower and more controlled reaction reducing the heating, and it avoids the ammonia gas during the setting [1]. The reaction process is given by the following equations (Eq 1):

$$\begin{gathered} KH_2PO_4\,(aq) \rightarrow K^+\,(aq) + H_2PO^{4-}\,(aq) \\ KH_2PO_4\,(aq) \rightarrow K^+\,(aq) + HPO_4^{2-}\,(aq) + H^+\,(aq) \\ KH_2PO_4\,(aq) \rightarrow K^+(aq) + PO_4^{3-}\,(aq) + 2H^+\,(aq) \end{gathered} \tag{1}$$

If ammonium phosphate is used, K^+ can be replaced by NH_4^+. MgO also dissociates in water according to the following equations (Eq 2) [8]:

$$\begin{gathered} MgO + H_2O \rightarrow MgOH^+ + OH^- \\ MgOH^+ + 2H_2O \rightarrow Mg(OH)_2 + H_3O^+ \\ Mg(OH)_2 \rightarrow Mg^{2+} + 2OH^- \end{gathered} \tag{2}$$

The dissociation of MgO through an acid-base reaction is due to the drop in pH [22]. The hydration of MPC is an exothermal reaction. When MgO and phosphate are slot together in the presence of mixing liquid, they react rapidly [2]. Generally, retarders are used to control the setting time of MPCs pastes hindering the contact of Mg^{2+} with phosphate cations (Eq 3) [4].

$$\begin{gathered} Mg^{2+} + 6H_2O \rightarrow Mg(H_2O)_6^{2+} \\ K^+ + Mg(H_2O)_6^{2+} + PO_4^{3-} \rightarrow MgKPO_4{\cdot}6H_2O \text{ (Final hydration form) [8]} \end{gathered} \tag{3}$$

The main reaction phase of MKPC K-struvite ($MgKPO_4{\cdot}6H_2O$) is accountable for the strength improvement [13]. The struvite is the main crystalline phase in MPCs and is a mineral family occurring in nature [1]. This crystal tends to precipitate from wastewater, and it is also used as

phosphate fertiliser [23]. Other hydration products are Scherlite [$(NH_4)_2Mg(HPO_4)_2 \cdot 4H_2O$], Ditmarite ($NH_4MgPO_4 \cdot H_2O$) and Stercorite ($NaNH_4HPO_4 \cdot 4H_2O$) [2].

The retarders generally employed are borax ($NaB_4O_7 \cdot 10H_2O$) [24–25]; sodium triphosphate (STP, $Na_5P_3O_{10}$), that increases the reaction time, maximising the workability and allowing the formation of schertelita phase [26–27]; boric acid (H_3BO_3) [28–29] and glacial acetic acid (CH_3COOH) [30]. Pozzolanic materials as fly ash (FA) [31–32], silica fume (SF) [33–34] and metakaolin [35], can be used as additives that lead to high-early strength, high workability, low porosity, water and chemical corrosion resistance. Different studies have been carried on reduction of brittleness through fibres used on MPC composition. For example, several matrixes have been prepared with the addiction of steel [36] and micro-steel fibres [37], glass fibres [38] and basalt fibres [33]. A very interesting property of MKPC conglomerates is the ability of bonding strength with various materials which allowed studies with natural fibres like coir fibre (CF) [39], corn stalk [40] or hemp [41]. These lightweight aggregate-based concretes improve the thermal and acoustic insulation parameters, reducing unit weight and costs.

As described above, several researches investigate the performance and properties of MKPC conglomerates. On the other hand, one of the shortcomings of the existing literature (addressed in the current study) concerns an in-depth investigation of the performance and potential of these types of conglomerates to be more sustainable (with the use of common and inexpensive materials), and sufficiently performing in a 3D printing construction process.

3. Materials and methods

3.1. Raw materials

The components for the preparation of the groups of samples are listed and described below (Table 1). Specifically, magnesium oxide, potassium dihydrogen phosphate, borax, fly ash, silica fume, water and aggregates were employed.

Table 1. Mix components.

Components		
Binder	MgO	Magnesium oxide
	KDP	Potassium dihydrogen phosphate
	FA	Fly ash
Additives	SF	Silica fume
		Borax
Water		
Aggregates		

The magnesium oxide is the decomposition product of magnesium carbonate over 500° [4]. The product used was MAGOX® Super Premium provided by Andrea Gallo Di Luigi S.r.l, Genova (Italy) and it is synthetic high-purity magnesium oxide obtained from deep well brine with a specific surface area of 150 m^2/g (the magnesia surface can influence the setting time [42]). We used Yara Tera KRISTA MKP provided by Yara Italia S.p.A, Milano (Italy) with phosphorus pentoxide P_2O_5 52% and potassium oxide K_2O 34%. The fly ash (Micro-pozz PFA) was provided by General Admixtures

S.p.A., Pozzano Veneto (Italy). FA is a by-product of coal-fired power generation. FA reduces the exothermic heat generated during early hydration, but it also increases the workability of fresh mixtures, the strength, the setting time, and MPC pastes flow ability. Silica fume (Micro-pozz DSF) was also provided by General Admixtures S.p.A., Pozzano Veneto (Italy). SF improves the bonding and abrasion strength, as well as the corrosive resistance against chemicals, yet it lowers permeability and the expansion thanks to the alkali-silica reaction phenomenon. Sodium borate tetrahydrate was provided by by Andrea Gallo Di Luigi S.r.l, Genova (Italy). Borax ($NaB_4O_7 \cdot 10H_2O$) mixed with phosphate is hydrolysed in the solution to yield $B_4O_7^{2-}$ ions. These react rapidly with Mg^{2+} ions to form compounds that precipitate as a film around the MgO grains. This film severely retards the reaction between the MgO and the phosphate [2]. The last components of the mix composition are water and fine sand with particle size 0.5–1 mm given that we cannot use excessively big particles in the printing process.

3.2. Specimen compositions

Four different groups of samples (in total twelve samples) were prepared and characterized to compare the different properties as a function of the composite modification. The starting mix composition was obtained with the following ratios (Eq 4):

$$\begin{gathered} \frac{\mathrm{KDP}}{(\mathrm{MgO+FA})} = 0.43 \\ \mathrm{MgO} = 40\%\ (\mathrm{FA} + \mathrm{MgO}) \\ \frac{Water}{Binder} = 0.83 \\ \frac{Aggregates}{Binder} = 0.45 \\ \frac{Borax}{(\mathrm{MgO} + \mathrm{FA})} = 4 \\ \mathrm{SF} = 10\%\ \mathrm{Binder} \end{gathered} \tag{4}$$

Samples 1, 2, 3, and 4 have the same composition but a different water-binder ratio, as illustrated in table 2, to evaluate the influence of water content on mechanical properties and found best composition considering the compromise between workability and resistance. Mix 5 and 6 are made replacing the FA content by weight with the same weight of SF. The future production of FA is correlated with the decommissioning of coal-fired plants. This implies that this material will be less and less available in the future. Therefore, the substitution with SF, which has pozzolanic properties too, is tested. As a strategy to reduce the environmental impact, aggregates can be replaced by recycled materials. Samples 7 and 8 have the same composition as sample 3 but the sand was replaced. Sample 7 contains recycled expanded glass (0.5–1 mm), instead sample 8 contains rubber granulate (0.5–1 mm) from tyre casings. Samples 9, 10, 11, and 12 have the same composition with lower borax content with respect to the former samples but a different water-binder ratio (Table 2). The component weights of all samples are summarised in Table 3.

Table 2. Mix compositions ratios.

Sample	$\frac{KDP}{(MgO+FA)}$	$\frac{MgO}{(FA+MgO)}$	$\frac{Borax}{(MgO+FA)}$	$\frac{SF}{Binder}$	$\frac{Aggregates}{Binder}$	$\frac{Water}{Binder}$
1	0.43	0.40	4.00	0.10	0.45	0.83
2	0.43	0.40	4.00	0.10	0.45	1.00
3	0.43	0.40	4.00	0.10	0.45	1.17
4	0.43	0.40	4.00	0.10	0.45	1.33
5	1.07	1.00	10.00	0.90	0.78	1.72
6	1.07	1.00	10.00	0.90	0.78	2.01
7	0.43	0.40	4.00	0.10	0.45 (glass)	1.17
8	0.43	0.40	4.00	0.10	0.45 (rubber)	1.17
9	0.43	0.40	1.00	0.10	0.45	0.30
10	0.43	0.40	1.00	0.10	0.45	1.00
11	0.43	0.40	1.00	0.10	0.45	0.83
12	0.43	0.40	1.00	0.10	0.45	0.60

Table 3. Mix compositions.

Sample	Binder			Borax	SF	Water	Aggregates	
	MgO	KDP	FA					
1	126 g	135 g	189 g	1259 g	45 g	375 ml	203 g	sand
2	126 g	135 g	189 g	1259 g	45 g	450 ml	203 g	sand
3	126 g	135 g	189 g	1259 g	45 g	525 ml	203 g	sand
4	126 g	135 g	189 g	1259 g	45 g	600 ml	203 g	sand
5	126 g	135 g	0 g	1259 g	234 g	450 ml	203 g	sand
6	126 g	135 g	0 g	1259 g	234 g	525 ml	203 g	sand
7	126 g	135 g	189 g	1259 g	45 g	525 ml	203 g	glass
8	126 g	135 g	189 g	1259 g	45 g	525 ml	203 g	rubber
9	126 g	135 g	189 g	315 g	45 g	135 ml	203 g	sand
10	126 g	135 g	189 g	315 g	45 g	450 ml	203 g	sand
11	126 g	135 g	189 g	315 g	45 g	375 ml	203 g	sand
12	126 g	135 g	189 g	315 g	45 g	270 ml	203 g	sand

3.3. Specimen characterization

As a first activity, powder materials were dry-mixed. MKPC mortars were prepared in an automatic mixer in conformity with UNI EN 196-1 [44]. A flow test was performed, according to UNI 7044, with a manual flow table, to evaluate the rheology of the fresh mixtures [43]. A cylindrical mould was placed at the centre of the flat plate and filled with mortar, then the mould was lifted and fifteen hits in fifteen seconds were applied. After the measurement of the initial diameter (Di) and final diameter (D) of the mixture, the flow values were calculated as follows (Eq 5):

$$\%flow = \frac{(D - D_i)}{D_i}\% \tag{5}$$

The percentage increase of the diameter represents the flow of a specimen.

Immediately after mixing, the mortars were placed into prismatic moulds (dimensions 40 × 40 × 160 mm). A comparison of the characteristics of identical samples showed that vibration is not needed due to the high fluidity. The flexural and compressive strengths were measured at 90 min and 7 d curing. Samples for compressive and flexural strength were tested by a MATEST device, Milan, Italy compliance with 89/392/CEE. The flexural tests were carried out with a loading rate in the range of 50 ± 10 N/s [44]. Every half part of broken samples from the flexural strength test was used for compressive strength test with a loading rate in the range of 2400 ± 200 N/s [44]. Each measurement was replicated, and the average value was taken as the value of strength.

Scanning electron microscopy (SEM) was employed to investigate the hydration products, microstructure, and porosity. Specimens for SEM analysis were first chopped and dried in an oven for 1h 30 min. For analysis, a FESEM-EDX Carl Zeiss Sigma 300 VP (Carl Zeiss Microscopy GmbH, Jena, Germany) electron microscope was used, and the samples were sputtered with gold after immobilization onto aluminium stubs (Sputter Quorum Q150 Quorum Technologies Ltd, East Sussex, UK). An optical microscope (premier series dyno-lyte portable microscope and background cold lighting) was employed to observe the surface break.

4. Results and discussion

4.1. Flow test and density

The increase of the water-binder ratio determines an increase of the flow values. The flow also depends on the type and on the total volume of the aggregates. Moreover, an increase of the water-binder ratio leads to a lower density of the consolidated specimens.

Samples 1 and 2 do not show significant differences, which instead become very relevant with higher water content (samples 3 and 4). Therefore, with a water/binder ratio more than 1 there is a significant increase in fluidity and consequently in repulsive rheological forces. Samples 5 and 6 have only silica fume which has a greater volume at the same weight than fly ash, for this reason, the cohesion forces increase considerably, and these samples are drier than the corresponding samples 2 and 3. Samples 7 and 8 result drier and with lower density and flow values with respect to the corresponding sample 3 due to the high volume of aggregate. Furthermore, sample 7, with expanded glass, has a greater volume of aggregate than rubber (sample 8), for this reason, the flow is lower, as well as the density is. Finally, samples 10, 11 and 12 also show that with the increase of water the flow increases too and density decreases. The influence of the decreasing of borax content is evident in sample 10 compared to sample 2, with a high increase in flow and decrease in density. The flow test results are summarised in Table 4 together with density values.

Table 4. Flow test values and density of the fresh and consolidated specimens.

Sample	Water	Flow test	Density
1	375 mL	35%	1325 kg/mc
2	450 mL	46%	1333 kg/mc
3	525 mL	300%	1250 kg/mc
4	600 mL	583%	1200 kg/mc
5	450 mL	9%	1100 kg/mc
6	525 mL	29%	1032 kg/mc
7	525 mL	23%	950 kg/mc
8	525 mL	39%	1120 kg/mc
10	450 mL	733%	1171 kg/mc
11	375 mL	567%	1331 kg/mc
12	270 mL	483%	1554 kg/mc

4.2. Surface break

Comparing the surface break of the specimens with different water-binder ratios, it is possible to note the variation of entrained air. From optical microscope observations the difference in distribution and size of the pores is clear. Indeed, with a lower content of water, the air content is relevant with large voids in the structure. On the contrary, increasing the ratio, the porosity seems to increase. Samples 1 and 2 have a similar porous structure, confirmed by the near-identical density values, with large gas bubbles probably due to the quite dry mixes. On the other hand, with a further increase of water content, the general porosity increases, also highlighted by a significant decrease in density, with smaller and more uniformly distributed gas bubbles. Figure 1 shows the big voids in samples 1 and 2. Sample 1 has a different coloration, greyer, probably due to a different reaction process in presence of a lower quantity of water. As from the apparent density, the increase of water content reduces the specific weight. This has an influence on the resistance as the next results will demonstrate.

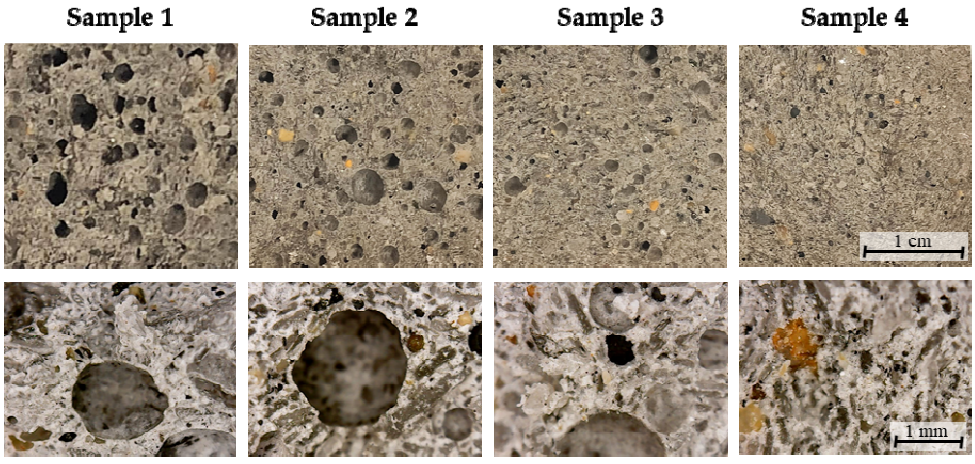

Figure 1. Sections of the specimens. Comparison of samples with different water-binder ratios.

Comparing specimens 5 and 6, there is no discernible difference between the two surface breaks.

The porosity of the specimen 7 and 8 can be compared with sample 3, but the inclusion of different aggregates is quite clear. Actually, expanded glass and rubber granulate are easily distinguishable and result homogenously distributed in the matrix.

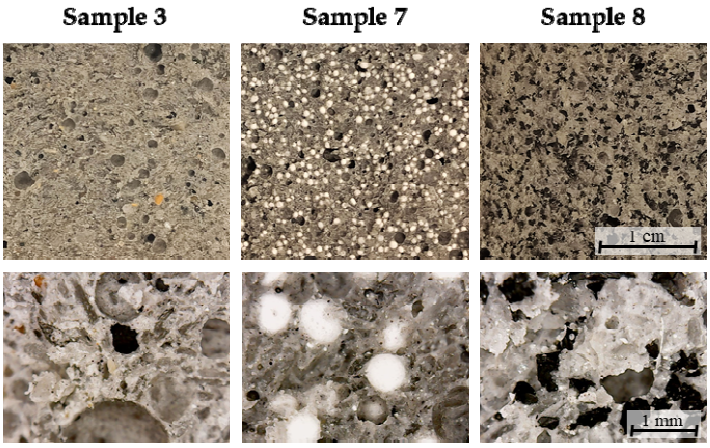

Figure 2. Comparison of the samples with different type of aggregate.

Sample 9 is not showed because extremely dry, and it cannot be employed for possible applications. Sample 10, 11 and 12 suggested the same observation on the influence of water on the porosity, as observed in the first four samples. In fact, with the increase of water, a decrease of density and increase of porosity can be observed.

4.3. Flexural and compressive strengths

Table 5 shows all the results of compressive and flexural strength tests of the mortars after 90 min and 7 d curing.

Table 5. Flexural and compressive strengths.

Sample	Flexural strength (MPa)		Compressive strength (MPa)	
	90 min	7 d	90 min	7 d
1	2.43 ± 0.12	1.88 ± 0.09	5.00 ± 0.25	6.44 ± 0.32
2	1.23 ± 0.06	1.71 ± 0.09	3.14 ± 0.16	5.73 ± 0.29
3	1.25 ± 0.06	1.56 ± 0.08	2.09 ± 0.10	4.59 ± 0.23
4	0.58 ± 0.03	1.09 ± 0.05	1.18 ± 0.06	2.76 ± 0.14
5	1.41 ± 0.07	1.35 ± 0.07	2.61 ± 0.13	4.77 ± 0.24
6	1.38 ± 0.07	1.29 ± 0.06	2.83 ± 0.14	4.97 ± 0.25
7	0.94 ± 0.05	1.63 ± 0.08	1.99 ± 0.10	4.80 ± 0.24
8	0.30 ± 0.02	1.32 ± 0.07	1.68 ± 0.08	3.23 ± 0.16
10	0.39 ± 0.02	1.24 ± 0.06	1.14 ± 0.06	4.78 ± 0.24
11	1.09 ± 0.05	1.76 ± 0.09	3.10 ± 0.16	7.18 ± 0.36
12	2.05 ± 0.10	1.62 ± 0.08	6.09 ± 0.30	9.98 ± 0.50

The results show a general brittle behaviour of materials. In fact, the flexural strength values are generally low with a limited increasing trend after 7 d, therefore the reduction in flexural strength found in samples 1 or 5 is probably due to experimental errors, being the flexural strength almost stable. On the contrary, the compressive strength increases due to the development of hydration products such as Struvite.

4.3.1. Sample 1 to 4: variation of water-binder ratio

Figure 3 shows an inverse relationship between compressive strength and water-binder ratio. This behaviour is predictable and common to all cement composites. The same observation concerns sample 10, 11 and 12, whereby lowering the water-binder ratio, the resistances, especially in compression, increase considerably. As mentioned above, the water-binder ratio has an impact on the specific weight, in fact, there is a directly proportional relationship between resistance and density.

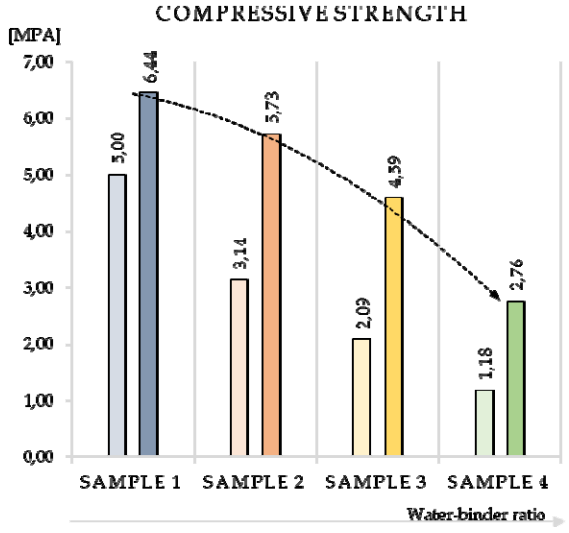

Figure 3. Variation of compressive strengths depending on the water-binder ratio. The values of each sample refer to 90 min (first column) and 7 d (second column).

4.3.2. Comparison of sample 2 and 5, 3 and 6: replacement of FA with SF

The comparisons are relative to samples with same content of water but with bare FA and with SF as FA replacement. Figures 4 and 5 show similar results, this can suggest a possible elimination of FA from MKPC mixtures, a material that will be unavailable in the future.

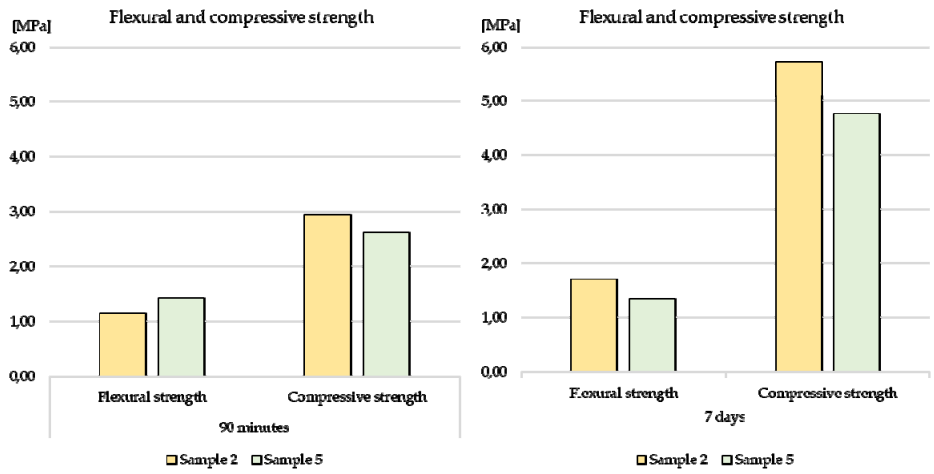

Figure 4. Variation of flexural and compressive strength with FA (sample 2) and with SF as FA replacement (sample 5), constant the water content (450 mL).

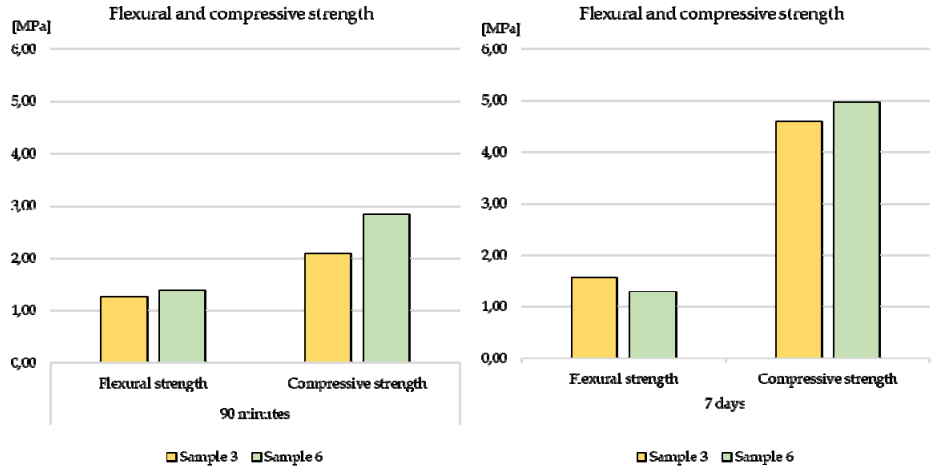

Figure 5. Variation of flexural and compressive strength with FA (sample 3) and with SF as FA replacement (sample 6), constant the water content (525 mL).

4.3.3. Sample 1, 7 and 8: variation of the type of aggregates

Figure 6 shows the compressive strengths values in case of sand, glass or rubber used as aggregates, keeping constant the other mixture parameters. The results are almost comparable. This evidence could support the use of recycled materials as sustainable strategy in construction. After analysis of the specific weight of samples 3 and 7, it is noted that with approximately the same compressive strength the sample with expanded glass is considerably lighter.

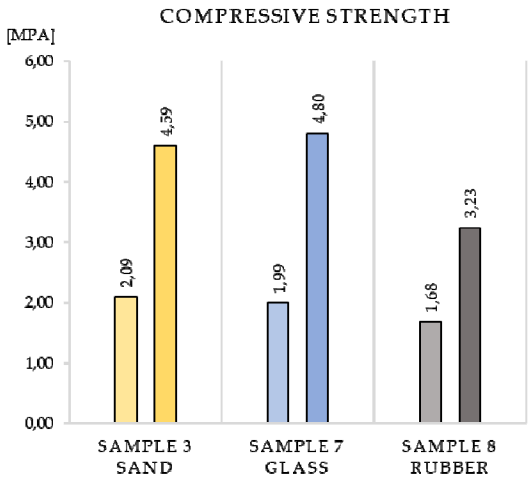

Figure 6. Variation of compressive strength with different types of aggregates. The values of each sample refer to 90 min (first column) and 7 d (second column).

4.3.4. Sample 1 and 11: variation of the content of borax

Figure 7 shows the compressive strengths values of sample 1 and 11 with different weight ratio of borax over the sum of magnesia and fly ash (4 and 1 respectively). What is expected is that by reducing the borax content the resistances would increase since, as previously reported, the action of the retarders affects the development of the struvite crystals responsible for the resistances [13]. The effect of the formation of struvite can be seen in this case because, despite sample 11 has a higher flow value due to the significantly lower quantity of borax, the density values in the consolidated specimens are similar due to the gradual formation of hydration products (k-struvite). K-struvite tends to increase the resistances of sample 11 which has higher compressive strength values at 7 days. For this reason, we must not only consider the flow but in this case especially the density of the hardened sample.

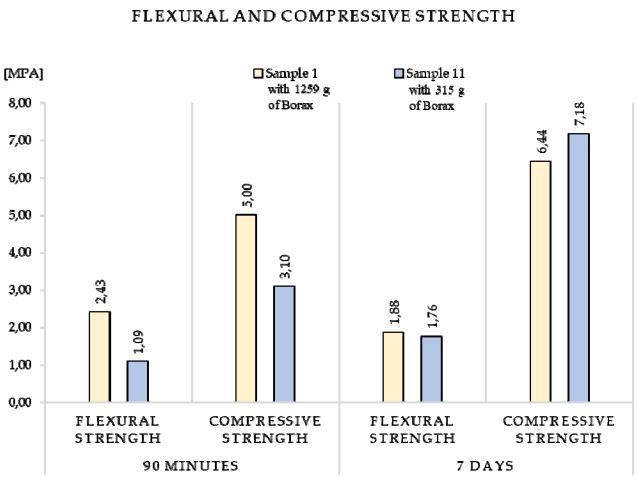

Figure 7. Variation of flexural and compressive strength with different content of borax. The water-binder ratio is 0.83 for each sample.

4.4. SEM analysis

In order to observe the main reaction products, the SEM analysis was performed on some samples.

Figure 8 shows a k-struvite crystal, largely present in all the samples analysed, and spherical elements, SF grains. As expected, the SF particles fill in the gaps of the structure increasing the density. A different microstructure and density can be observed after comparison of samples 2 and 10 detections. Figure 9 shows the SEM images of the samples prepared with the same content of water, but a different content of borax. The presence of this kind of retarder, used to regulate the reactions and setting time, involves the reduced development of the microstructure. Therefore sample 10 shows a more compact structure.

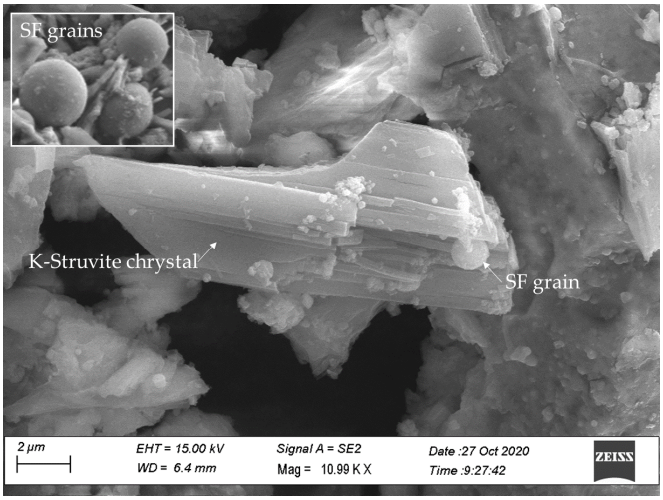

Figure 8. Sample 2: k-struvite crystal, largely present in all the samples analysed and SF grains.

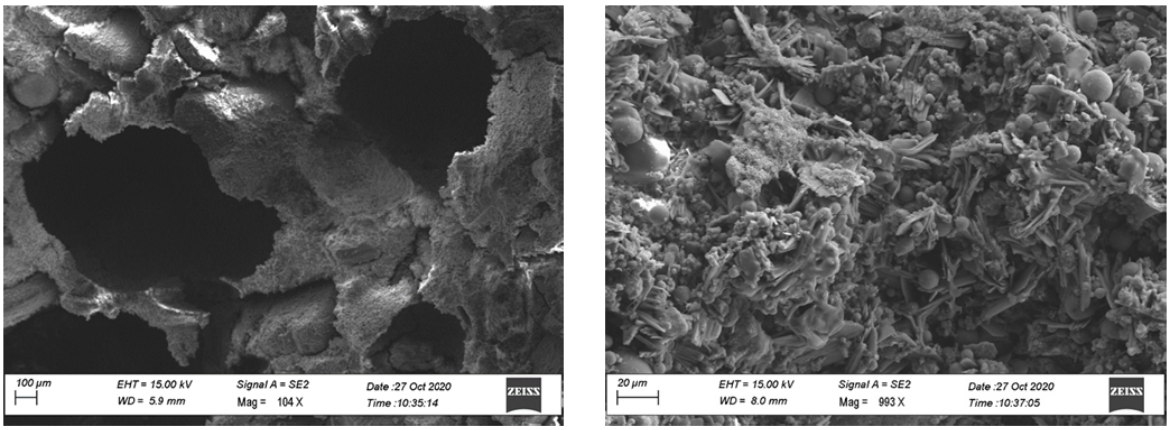

(a) (b)

Figure 9. Comparison of the samples with different content of borax: (a) sample 2 with more borax; (b) sample 10 with less borax.

The expanded recycled glass beads (visible in Figure 10), has good adhesion to the cement

matrix. In literature, it is possible to observe cases in which the recycled glass sphere breaks showing the beehive structure, but despite the strength tests carried out, the sphere is not broken [45]. This condition is also visible in other overviews. The explanation can be found in the fact that in traditional mixtures the resistance of the sphere is lower than the resistance of the interface between the cement matrix and the glass. On the contrary, in the present case the resistance of the interface is lower than the resistance of the glass. The surface of the rubber granulate is smooth and with hydrophobic characteristics accordingly it has not a good adhesion as shown in the Figure 8 where the voids between the aggregate and the cement matrix is visible.

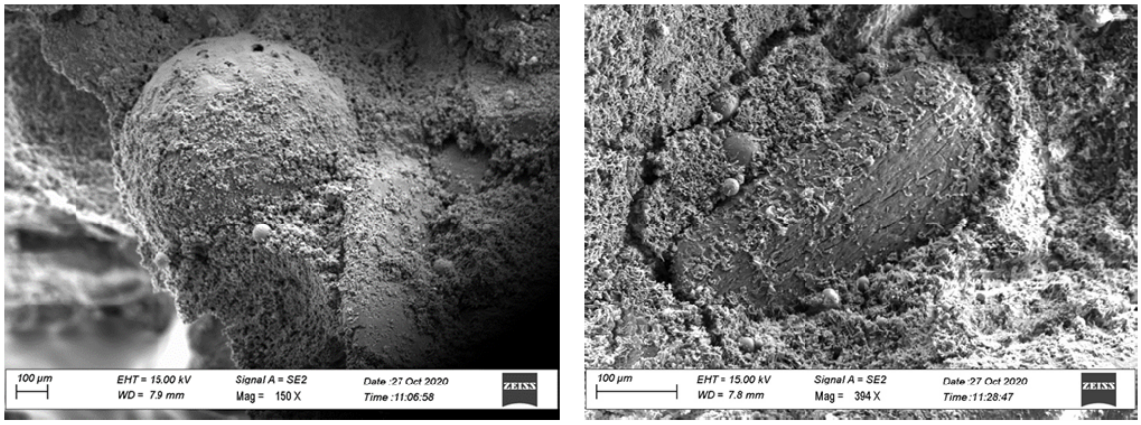

Figure 10. Comparison of (a) sample 7 with expanded glass, (b) sample 8 with rubber aggregates.

4.5. Discussion

The first reflection on the results obtained in laboratory concerns the influence of the water content on the workability. The greater amount of water content involves not only more fluidity, but also determines a density decrease due to the formation of a porous structure. Further clarification of the real density in this regard can be given by future analyses of the samples.

The result of compressive strength at 90 minutes of sample 1 (5.00 MPa) is comparable with the compressive strength of sample M40FA60S10-4 (5.36 MPa) from another study, although the composition of the two specimens is different in the water content (the water-binder ratio is 0.83 and 0.3 respectively). The mix composition of sample M40FA60S10-4 is composed of the following ratios: The sand-to-binder ratio was 0.45; the water-to-binder ratio was 0.3; the mass ratio of KDP over the sum weight of magnesia and fly ash was 0.43; the weight ratio of borax over the sum of magnesia and fly ash was 4 and silica fume was 10% as the weight ratio of the binder [13].

Reducing the weight ratio of borax over the sum of magnesia and fly ash from 4 to 1, the workability completely changes. In fact, comparing samples 10 and 11 with samples 2 and 1 respectively, at equal water content, an extremely high fluidity can be observed. This is due to the net reduction in the overall amount of borax that absorbs part of the mixing water. As hypothesized, setting times are also significantly reduced, making application difficult if not controlled. Comparing the resistances of samples 1 and 11 it can be expected that the resistances of the sample with less borax would be higher because of the formation of a greater quantity of struvite crystals. This effect

starts at 7 d curing (compressive strength at 7 d).

With the replacement of FA with SF there is an important change of workability. In fact, with the same water content, the SF specimens result extremely dry. This can be caused by the influence of the different density on workability. Instead, the variation of the resistances is minimal, and these results can be considered very important in light of a more sustainable production of environmental safe conglomerates without the use of fly ash. In this respect, it is also interesting to consider the results obtained with samples 7 and 8 which are characterized by the presence of recycled materials such as glass and rubber as aggregates. Having carried out a weight replacement, these types of specimens show lightness and thermo-insulating properties.

Therefore, for all these samples, there are many advantages from a sustainable point of view, namely the elimination of toxic compounds as fly ash; the use of recycled and thermo-insulating materials with the possibility of reusing products at the end of their life as aggregates for new cementitious products; the presence of struvite which could increase their resistance. Moreover, struvite constitutes a soil improver and in magnesium phosphate cements it is produced in large quantities [46]. For this reason, a study that evaluates the possibility of adding the soil with extracts of disused cement products would be interesting. Future developments of these types of conglomerates will be devoted to the preparation and characterization of materials which are characterized at the same time of bare silica fume, waste aggregates and low borax.

The 3D printing cement materials developed in the last years have reached high performance in terms of mechanical properties. However, these results cannot be compared with the current research focused on printable MKPC mortars. For example, the compressive strength after seven days of curing of an alkali-activated composite can reach about 60 MPa [18] and the mechanical properties can be further improved using fibres, that influence especially the flexural strength [17,19,20]. As the results show, the developed materials are almost brittle, therefore a future investigation can be focused on the incorporation of fibres.

The flow test results of some of the samples guarantee the workability requirements stated. A future objective can be the increasing of flowability of 10% using dispersant additives without the reduction of more than 5% of resistances.

4.5.1. Best MKPC composition and guidelines for practical applications.

The experimentation conducted offers a wide range of samples. Therefore, a broad spectrum of types of workability has been evaluated. As a result, some of the samples can be considered for experimentation in 3D printing. In fact, by excluding the more fluid or less workable types for each type of mixture made, an appropriate level of workability for the standards of 3D printing was reached. Furthermore, the setting times are assumed to guarantee the creation of consecutive layers avoiding the collapse. Specifically, a good compromise between the characteristics of plasticity, fluidity, workability and setting times is achieved by sample 2 characterised by a water-binder ratio equal to 1. The sample also reaches a compressive strength of about 3 MPa in 90 min of maturation which is assumed to be a sufficient result for the extrusive printing process. The study on the application of potassium magnesium phosphate cement for 3D printing mentioned takes as a reference the compressive strength values of 1 MPa at 20 min and 4.93 MPa at one day as sufficient for most of the requirements of 3D printing mortars. Another mixture that could be interesting for application in the printing of cementitious materials is sample 7 with expanded recycled glass.

Although the resistances reached at 90 min are lower (about 2 MPa), the use of recycled materials as aggregates and the insulating properties would allow a new and broad spectrum of applications.

To provide some practical guidelines for the preparation of the conglomerates for 3D printers, the following suggestions are proposed to reproduce the investigated composites (sample 2 or 7). Firstly, dry-mix powder materials by hand while adding them one at a time. Then mix through an automatic mixer, in conformity with UNI EN 196-1, for at least 15 seconds. Add the recommended quantity of water and continue the mechanical mixing. During this process, it is important to pay attention to the setting time, so as to prevent reactions from starting before the placing into the tank. Using lightweight aggregates, such as sample 7 with glass, take notice of the difference in volume weight ratio being equal. After these simple steps the conglomerate is ready to be loaded into the tank of a 3D printer.

5. Conclusions

The present research investigated the use of magnesium potassium phosphate cement for innovative composites which showed interesting results both for extrusive 3D printing applications and environmentally sustainable applications. The novelty of the proposed research involves three aspects: (i) different chemical admixtures with lightweight aggregates are proposed with the objective of achieve good performances compatible with 3D printing, (ii) an innovative composition is proposed to demonstrate the possible replacement of fly ash with silica fume in the preparation protocol by maintaining the same performances of traditional MPC, (iii) specific guidelines are developed to support stakeholders in the reproduction of the proposed composites in the most performing chemical admixture configurations.

During the investigation, twelve different chemical admixtures have been proposed and tested for different characteristics: setting time; early strength; flexural and compressive strength; effective bonding and drying shrinkage. Among the investigated samples, two configurations have been identified demonstrating their sustainability and effective performances suitable to be used with the additive manufacturing technology. In particular, the two chemical admixtures (sample 2 and 7) are reported in the following:

i. Sample 2 is composed by a sand-to-binder ratio of 0.45. Moreover, the water-to-binder ratio is 1.00 and the mass ratio of KDP over the sum weight of magnesia and fly ash is 0.43. The weight ratio of borax over the sum of magnesia and fly ash is 4 and silica fume is 10% as the weight ratio of the binder.
ii. In sample 7, the glass aggregates-to-binder ratio is 0.45, the water-to-binder ratio is 1.17 and the mass ratio of KDP over the sum weight of magnesia and fly ash is 0.43. The weight ratio of borax over the sum of magnesia and fly ash is 4 and silica fume is 10% as the weight ratio of the binder.

In conclusion, the proposed research can be useful both for increase the knowledge of theoretical research on magnesium potassium phosphate cement conglomerates, and for practical support of technicians who intend to use high performances 3D printable materials. Future research will develop a high-performance 3D printed building component with the investigated chemical admixtures of magnesium potassium phosphate cement to be used in a new conceptual design of the building construction process. In particular, the research will be focused on the improvement of the proposed admixtures, through several printing tests, in relation to the extrusion system and the 3D

printer requirements.

Acknowledgments

The authors would like to thank Dr. Adriano Boghetich for the help in the preparation and characterization of the specimens.

Conflict of interest

The authors declare no conflict of interest.

References

1. Walling SA, Provis JL (2016) Magnesia-based cements: a journey of 150 years, and cements for the future? *Chem Rev* 116: 4170–4204.
2. Haque MA, Chen B (2019) Research progresses on magnesium phosphate cement: A review. *Constr Build Mater* 211: 885–898.
3. De Schutter G, Lesage K, Mechtcherine V, et al. (2018) Vision of 3D printing with concrete-technical, economic and environmental potentials. *Cement Concrete Res* 112: 25–36.
4. Yang N, Shi C, Yang J, et al. (2014) Research progresses in magnesium phosphate cement-based materials. *J Mater Civil Eng* 26: 04014071–04014078.
5. Kouassi M, Michaïlesco P, Lacoste-Armynot A, et al. (2003) Antibacterial effect of hydraulic calcium phosphate cement for dental applications. *J. Endodont* 29: 100–103.
6. Zhao Y, Yu S, Wu X, et al. (2021) Construction of macroporous magnesium phosphate-based bone cement with sustained drug release. *Mater Design* 200: 109466.
7. Qiao F, Chau C K, Li Z (2010) Property evaluation of magnesium phosphate cement mortar as patch repair material. *Constr Build Mater* 24: 695–700.
8. Park JW, Kim KH, Ann KY (2016) Fundamental properties of magnesium phosphate cement mortar for rapid repair of concrete. *Adv Maters Sci Eng* 2016: 1–7.
9. Li J, Zhang W, Cao Y (2014) Laboratory evaluation of magnesium phosphate cement paste and mortar for rapid repair of cement concrete pavement. *Constr Build Mater* 58: 122–128.
10. Iyengar SR Al-Tabbaa A (2007) Developmental study of a low-pH magnesium phosphate cement for environmental applications. *Environ Technol* 28: 1387–1401.
11. Singh D, Wagh AS, Cunnane JC, et al. (2008) Chemically bonded phosphate ceramics for low-level mixed-waste stabilization. *J Environ Sci Heal A* 322: 527–541.
12. Liu Y, Kumar S, Kwang JH, et al. (2013) Magnesium ammonium phosphate formation, recovery and its application as valuable resources: A review. *J Chem Technol Biot* 88: 181–189.
13. Weng Y, Ruan S, Li M, et al. (2019) Feasibility study on sustainable magnesium potassium phosphate cement paste for 3D printing. *Constr Build Mater* 221: 595–603.
14. Roussel N (2018) Rheological requirements for printable concretes. *Cement Concrete Res* 112: 76–85.
15. Chougan M, Ghaffar SH, Jahanzat M, et al. (2020) The influence of nano-additives in strengthening mechanical performance of 3D printed multi-binder geopolymer composites. *Constr Build Mater* 250: 118928.

16. Bong SH, Nematollahi B, Nazari A, et al. (2019) Method of optimisation for ambient temperature cured sustainable geopolymers for 3D printing construction applications. *Materials* 12: 902.
17. Nematollahi B, Vijay P, Sanjayan J, et al. (2018) Effect of polypropylene fibre addition on properties of geopolymers made by 3D printing for digital construction. *Materials* 11: 2352.
18. Chougan M, Ghaffar SH, Sikora P, et al. (2021) Investigation of additive incorporation on rheological, microstructuraland mechanical properties of 3D printable alkali-activated materials. *Materi Design* 202: 109574.
19. Panda B, Paul SC, Tan MJ (2017) Anisotropic mechanical performance of 3D printed fiber reinforced sustainable construction material. *Mater Lett* 209: 146–149.
20. Bos FP, Bosco E, Salet TAM (2019) Ductility of 3D printed concrete reinforced with short straight steel fibers. *Virtual Phys Prototy* 14: 160–174.
21. Cuevas K, Chougan M, Martin F, et al. (2021) 3D printable lightweight cementitious composites with incorporated waste glass aggregates and expanded microspheres—Rheological, thermal and mechanical properties. *J Build Eng* 44: 102718.
22. Soudée E, Péra J (2000) Mechanism of setting reaction in magnesia-phosphate cements. *Cement Concrete Res* 30: 315–321.
23. Rahman MM, Mohd MA, Rashid U, et al. (2013) Production of slow release crystal fertilizer from wastewaters through struvite crystallization—A review. *Arab J Chem* 7: 139–155.
24. Sugma T, Kukacka LE (1983) Characteristics of magnesium polyphosphate cements derived from ammonium polyphosphate solutions. *Cement Concrete Res* 13: 499–506.
25. Sugma T, Kukacka LE (1983) Magnesium monophosphate cements derived from diammonium phosphate solutions. *Cement Concrete Res* 13: 407–416.
26. Ribeiro DV, Agnelli JAM, Morelli MR (2013) Study of mechanical properties and durability of magnesium phosphate cement matrix containing grinding dust. *Mater Res* 16: 1113–1121.
27. Ma C, Liu y, Zhou H, et al. (2021) Influencing mechanism of sodium tripolyphosphate on the rheological properties of magnesium phosphate cement. *Powder Technol* 387: 406–414.
28. Ribeiroa DV, Paulab GR, Morelli MR (2019) Effect of boric acid content on the properties of magnesium phosphate cement. *Constr Build Mater* 214: 557–564.
29. Lahalle H, Coumes CCD, Mesbah A, et al. (2016) Investigation of magnesium phosphate cement hydration in diluted suspension and its retardation by boric acid. *Cement Concrete Res* 87: 77–86.
30. Jun L, Ji YS, Huang GD, et al. (2017) Retardation and reaction mechanisms of magnesium phosphate cement mixed with glacial acetic acid. *RSC Adv* 7: 46852–46857.
31. Jianming Y, Luming W, Cheng J, et al. (2020) Effect of fly ash on the corrosion resistance of magnesium potassium phosphate cement paste in sulfate solution. *Constr Build Mater* 237: 117639.
32. Sun S, Liu R, Zhao X, et al. (2019) Investigation on the water resistance of the fly-ash modified magnesium phosphate cement. *IOP Conf Ser Mater Sci Eng* 587: 012007.
33. Ahmad MR, Chen B (2018) Effect of silica fume and basalt fiber on the mechanical properties and microstructure of magnesium phosphate cement (MPC) mortar. *Constr Build Mater* 190: 466–478.
34. Xu X, Lin X, Pan X, et al. (2020) Influence of silica fume on the setting time and mechanical properties of a new magnesium phosphate cement. *Constr Build Mater* 235: 117544.

35. Lu X, Chen B (2016) Experimental study of magnesium phosphate cements modified by metakaolin. *Constr Build Mater* 123: 719–726.
36. Frantzis P, Baggott R (2000) Bond between reinforcing steel fibres and magnesium phosphate/calcium aluminate binders. *Cement Concrete Comp* 22: 187–192.
37. Feng H, Sheikh MN, Hadi MNS, et al. (2018) Mechanical properties of micro-steel fibre reinforced magnesium potassium phosphate cement composite, mechanical properties of micro-steel fibre reinforced magnesium potassium phosphate cement composite. *Constr Build Mater* 185: 423–435.
38. Fang Y, Chen B, Oderji SY (2018) Experimental research on magnesium phosphate cement mortar reinforced by glass fiber. *Constr Build Mater* 188: 729–736.
39. Jiang Z, Zhang L, Geng T, et al. (2020) Study on the compressive properties of magnesium phosphate cement mixing with eco-friendly coir fiber considering fiber length. *Materials* 13: 3194.
40. Ahmad MR, Chen B, Oderji SY, et al. (2018) Development of a new biocomposite for building insulation and structural purpose using corn stalk and magnesium phosphate cement. *Energ Buildings* 173: 719–733.
41. Del Valle-Zermeño R, Aubert JE, Laborel-Préneron A, et al. (2016) Preliminary study of the mechanical and hygrothermal properties of hemp-magnesium phosphate cements. *Constr Build Maters* 105: 62–68.
42. Soudée E, Péra J (2002) Influence of magnesia surface on the setting time of magnesia-phosphate cement. *Cement Concrete Res* 32: 153–157.
43. Italian Organization for Standardization (UNI). Determination of consistency of cement Mortars using a flow table. UNI 7044:1972. Available from: http://store.uni.com/magento-1.4.0.1/index.php/uni-7044-1972.html.
44. Italian Organization for Standardization (UNI). Methods of testing cement—Part 1: determination of strength. EN 196-1. Available from: http://store.uni.com/magento-1.4.0.1/index.php/en-196-1-2016.html.
45. Petrella P, Di Mundo R, De Gisi S, et al. (2019) Environmentally sustainable cement composites based on end-of-life tyre rubber and recycled waste porous glass. *Materials* 12: 3289.
46. Rahman MM, Liu Y, Kwag JH, et al. (2011) Recovery of struvite from animal wastewater and its nutrient leaching loss in soil. *J Hazard Mater* 186: 2026–2030.

AIMS Press